ACS OMEGA

http://pubs.acs.org/journal/acsodf

Article

Study of Butylated Hydroxytoluene Inhibiting the Coal Oxidation at Low Temperature: Combining Experiments and Quantum Chemical Calculations

Yujia Huo, Hongqing Zhu,* and Xin He

Cite This: *ACS Omega* 2022, 7, 18552−18568

Read Online

ACCESS | Metrics & More | Article Recommendations

ABSTRACT: In order to cut off the chain reaction in the process of coal oxidation at low temperature (COLT), butylated hydroxytoluene (BHT) was used as an inhibitor to explore its inhibition effect and mechanism. In this paper, in situ Fourier transform infrared spectroscopy, electron paramagnetic resonance, and gas production of COLT experiments were conducted to compare the inhibited coal sample (BHT-Coal) with the raw coal. The results showed that BHT can effectively inhibit the formation of active free radicals, reduce the content of active alkoxy, carbonyl, and hydroxyl groups, increase the production temperature of CO, CO_2, and C_2H_4, and reduce the concentration. The crossing point temperature increased from 132.3 to 157.4 °C, indicating that BHT can reduce the spontaneous combustion tendency of the raw coal. To explore the inhibition mechanism of BHT on COLT, five typical active free-radical models were established, and their active sites, active bonds, and thermodynamic parameters were calculated according to the density functional theory. The results showed that the highly active H atoms of the phenolic hydroxyl group in BHT can combine with active free radicals to generate stable compounds, and the activation energy of each reaction is small, which can occur under normal temperature and pressure. The inhibition mechanism of BHT is to reduce the concentration of the free radicals, so as to weaken the chain reaction strength during the COLT. This study provides a reference for the development and utilization of inhibitors.

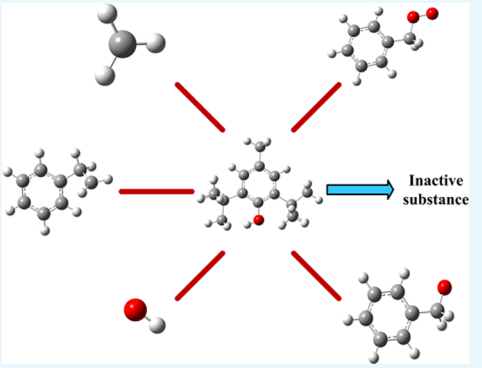

1. INTRODUCTION

At present, the coal is still the main production energy and raw material in the world, accounting for 30% of the world's energy consumption, while Asia's coal consumption accounts for about 75% of the world.[1,2] China is rich in coal resources, accounting for more than 67.5% of disposable energy, but the quality is poor. The low-grade coal is about 190 billion tons, accounting for 41.18% of the total coal reserves.[3−6] Coal spontaneous combustion is a common disaster phenomenon in the process of coal mining, storage, and utilization. Coal spontaneous combustion will produce toxic and harmful gases such as CO, CO_2, SO_2, and NO. Serious coal spontaneous combustion disaster will even cause coalfield fire and gas explosion, which poses a major threat to property and the safe production of coal mines.[7−10]

The process of coal spontaneous combustion is very complex. For a long time, scholars have carried out a lot of research on the mechanism of coal spontaneous combustion, and coal-oxygen compound theory has been most widely recognized. The theory holds that coal spontaneous combustion is caused by coal oxidation at low temperature (COLT), which is due to the physical adsorption,[11] chemical adsorption,[12] and oxidation at room temperature.[4,13] When the heat accumulates and cannot dissipate in time, the coal spontaneous combustion occurs.[14−16] On the basis, Li[17,18] put forward the theory of the free-radical reaction in 1996 and predicted the gas production mechanism in the process of COLT, and he believed that the active groups in coal can produce active free radicals and react with oxygen after fracture, resulting in COLT. Wei[19] used the electron spin resonance technology to determine the change law of free radicals under different coal types and fragmentation degrees and deduced the chain reaction mechanism of COLT. The results showed that O_2, moisture, light, and inorganic component content play an important role in the transmission of the free-radical reaction and put forward a new idea to inhibit COLT. Wang[20,21] proposed the elementary reaction sequence of each active group and successfully applied it to the identification of coal spontaneous combustion tendency. Qi et

Received: March 1, 2022
Accepted: May 13, 2022
Published: May 24, 2022

Table 1. Proximate Analysis and Ultimate Analysis of Coal[a]

proximate analysis				ultimate analysis				
M_{ad} (%)	A_{ad} (%)	V_{ad} (%)	FC_{ad} (%)	C (%)	H (%)	O (%)	N (%)	S (%)
9.78	17.47	41.02	31.73	55.39	3.18	16.53	0.36	0.77

[a]ad, air dry basis; *M*, moisture; *A*, ash; *V*, volatile matter; and FC, fixed carbon.

al. proposed the oxidation reaction pathways of alkyl groups,[22] carboxyl groups,[23,24] hydroxyl groups,[25] sulfur-containing groups,[26] and active free radicals,[27] which is helpful to deeply reveal the mechanism of COLT. Zhu applied the quantum chemistry method to predict the reaction pathways of original aldehyde[28] and hydroxyl groups[29] at different positions of coal molecules and calculated the thermodynamic parameters, which provided a theoretical basis for the research and development of inhibitors.

In order to inhibit the coal spontaneous combustion, the inhibitors are widely used. At present, common inhibitors are mud, three-phase foam, sodium silicate gel, and halogen salt solution,[30−32] whereas halogen salt solution mainly includes MgCl, CaCl, NaCl, and Na_2NO_3, which are widely used because of its low cost.[33−36] After the halogen salt solution is sprayed on the coal surface, due to its strong moisture absorption, a liquid film can be formed on the surface of coal particles to isolate oxygen and active groups. At the same time, it can also accelerate the heat released by coal oxidation through moisture evaporation. However, the use of halogen salt solution has been gradually reduced because they easily generate HCl and other toxic gases at high temperature, which is very harmful to the human body and the environment.[37] Scholars have found that some antioxidants used in the rubber industry can cut off the chain reactions of COLT. Zhan[38,39] applied the thermal analysis technology to explore the influence of ammonium on the COLT process, and the results showed that ammonium has high reaction activity, which can effectively eliminate free radicals on the coal surface to inhibit the chain reactions. Ma et al.[40] mixed poly (acrylic acid)/sodium alginate super absorbent (PS), ascorbic acid (VC), and moisture to gain a slow-release inhibitor, then the results indicated that it can reduce heat accumulation and cut off chain reactions, showing an obvious synergistic effect. Dou[41] found that ethylene glycol can not only form a protective film on the surface of coal particles to isolate oxygen but also provide H atoms to react with active free radicals to generate stable compounds and cut off the chain reactions. Xi[42−44] put forward an innovative technology of the complex antioxidant enzyme inhibitor and found that the mixture of polyethylene glycol-Cu, Zn superoxide dismutase, Mn catalase, and sodium dodecyl sulfate has good wettability and inhibition. Li[45,46] analyzed the inhibition effects of six antioxidants. He found that 2,2,6,6-tetramethyl-1-piperidinyloxy can combine with alkyl free radicals to reduce the activity.

Generally speaking, the traditional inhibitors have low cost and wide application and play a positive role in controlling the COLT to a certain extent. Their inhibition mechanism is to destroy the active structures and absorb water to isolate the oxygen, which is not based on the reaction mechanism of the COLT. Therefore, they cannot inhibit the COLT effectively, and some will even accelerate the process of water loss on the coal surface. The inhibition mechanism of antioxidants is to reduce the production of free radicals in the process of COLT and weaken the thermal effect, which can inhibit the COLT at the root.

Butylated hydroxytoluene (BHT) is a phenolic antioxidant with the largest production yield in recent years. It is often used as food additive to delay food rancidity with the characteristics of low cost, easy access, and high safety level, and it can be used as a proton donor to combine with active free radicals to make them inactive.[46,47] In this paper, BHT was selected as the inhibitor to explore its inhibition characteristics of coal spontaneous combustion. The distribution of active groups and gas production at different temperatures were analyzed by in situ Fourier transform infrared spectroscopy (in situ FTIR), electron paramagnetic resonance (EPR), and gas production experiments. Then, five typical active free-radical models were constructed. The reaction pathways and thermodynamic parameters of BHT and coal molecular active radicals were calculated using the quantum chemical method, and the inhibition mechanism was revealed.

2. EXPERIMENTS AND CALCULATION METHODS

2.1. Experiments. *2.1.1. Coal Samples and Inhibitor Preparation.* Lignite has low metamorphic degree, rich active groups, and high spontaneous combustion tendency, which is very suitable for this study.[48] Therefore, the coal sample selected is Xilin Gol League lignite, and the proximate and ultimate analysis results are shown in Table 1. First, under the protection of N_2, the outer part of a large fresh coal lump was removed, then the core was broken and sieved to obtain pulverized coal with size of 200−250 mesh. Second, the treated pulverized coal was put into a vacuum drying oven and dried at 40 °C for 48 h. Finally, the dried pulverized coal was put into a glass bottle for standby.

The solution mixing method was selected to prepare the inhibited coal sample (BHT-Coal). Since BHT is insoluble in water, 95% ethanol (hereinafter referred to as ethanol) was selected as the solvent.[47] Under a N_2 atmosphere, 19 mg of dry pulverized coal and 1 mg of BHT were weighted and fully mixed in 20 ml ethanol to stir evenly; as a control, the same method was selected to treat the dried raw pulverized coal. Both samples were left in a cool place for 24 h to fully precipitate and then were moved to a vacuum drying oven for 48 h. After the ethanol in the samples was completely evaporated, they were taken out and sealed for storage.

2.1.2. Examination of the Micromorphology. The scanning electron microscopy experiments were applied to characterize the micromorphology of the samples by a Zeiss supra 55 instrument. Before the experiments, the samples were plated with gold to make the surface of the samples conductive.

2.1.3. In Situ FTIR Test. The raw coal and BHT-coal samples were tested using the Thermo IS 50 in situ Fourier infrared spectrometer. In order to eliminate the interference of the diluent, the base vector of pure potassium bromide (KBr) was collected in the diffuse reflection test mode as a reference. The 0.001 g of the sample was weighted to mix with KBr powder in the ratio of 1:150 and ground for 20 min. The fully ground powder was pressed at 10 MPa for 1 min, then a transparent sheet with a diameter of 0.9 mm and a thickness of 0.1 mm was

https://doi.org/10.1021/acsomega.2c01229
ACS Omega 2022, 7, 18552−18568

obtained and was put into the reaction tank. The wavenumber range was 4000−400 cm^{-1}, the resolution was 4.0 cm^{-1}, and the cumulative scanning times were 64. During the test, dry air was continuously introduced with a flow rate of 60 ml/min, the test temperature range was 30−240 °C, the heating rate was 2 K/min, and the data were collected when the temperature rose to 30, 60, 90, 120, 150, 180, 210, and 240 °C.

2.1.4. EPR Test. According to EPR detection, free radicals, transition metals, lattice defects, and paramagnetic molecules such as O_2 and CO_2 can be analyzed.[49] In this paper, EPR was applied to detect the total concentration of free radicals in raw coal and BHT-Coal samples at different temperatures to compare and analyze the inhibition effect of BHT. The tests were carried out on the Bruker EMXplus EPR tester. Because the peak shape and g value of the solid-state EPR spectrum of 1,1-diphenyl-2-trinitrophenylhydrazine (DPPH, g = 2.0036) were similar to those of coal, it was used as the standard sample of solid free radicals in this experiment.[50] After 20 mg of DPPH was weighted for EPR benchmark calibration, 20 mg of raw coal and BHT-coal samples were weighted to raise the temperature to 40, 60, 90, and 120 °C, respectively, for detection. The instrument parameters were set as follows: the microwave frequency was 9.8 ± 10^{-8} GHz, microwave power was 4 mW, the central magnetic field was 3510 ± 10^{-6} G, the scanning width was 100 G, the time constant was 5.12 ms, the scanning time was 20.97 s, the modulation amplitude was 1 G, and the modulation frequency was 100 kHz. It should be noted that in order to ensure the uniformity of the experimental results, the depth of the sample tube inserted into the resonant cavity during measurement was 6 cm.

2.1.5. Gas Production Experiments of COLT. During the COLT, a variety of gases will be produced, such as CO, CO_2, C_2H_4, CH_4, H_2, and so on. The generation law of these gases changes with the coal samples.[51] The experimental device is composed of a reaction furnace with programmable temperature rise and a meteorological chromatograph. As shown in Figure 1, the gas generated during the temperature rise can be directly sent to the meteorological chromatograph for detection and recording. The 150 g of the prepared sample was weighted and put into the reaction furnace, and a thermocouple was arranged in the center of the sample to monitor the temperature. During the experiment, pure air was continuously introduced with a flow rate of 60 ml/min. The reaction furnace was heated from room temperature to 200 °C by using the programmable temperature rise, and the temperature rise rate is 2 K/min. During the heating process, every time the sample rose by 5 K, the gas generated was sent to the gas chromatograph to detect. CO, CO_2, and C_2H_4 were the most obvious index gases, so they were selected as the indexes to evaluate the oxidation degree of coal. It should be noted that the program was kept at a constant temperature for 20 min in every detection to ensure the accuracy of the detection.

In the initial stage of heating up, the central temperature of the sample is lower than that of the reaction furnace. Then, with the heat transfer of the equipment and the oxidation heat release of coal, the central temperature of the sample rises, and the heating rate increases with the increase in oxidation degree. At a certain time, the central temperature must be higher than that of reaction furnace, and the corresponding temperature is called cross-point temperature (CPT).[52] The CPT can reflect the difficulty of the sample oxidation reaction and can be used as an auxiliary index to judge the inhibition ability of antioxidants. The higher the CPT is, the less self-heating of coal is, the smaller the spontaneous combustion tendency is, and the better the inhibition ability of antioxidants is.

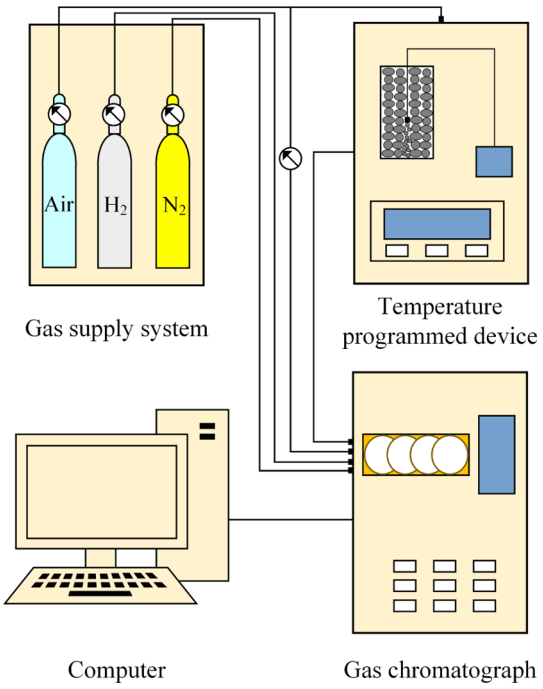

Figure 1. Experimental devices and processes.

2.2. Quantum Chemical Calculation Method. All models in this paper were established on Gauss View 6.0 software, and density functional theory (DFT) in Gaussian 16W was used for calculation.

2.2.1. Computational Contents. At normal temperature and pressure, only some active structures in coal molecules can chemically adsorb and react with oxygen, which are called active groups, mainly including alkyl functional groups (−CH, $-CH_2$, and $-CH_3$) and oxygen-containing functional groups (−OH, −C═O, −COOH and −CHO). Not only the original functional groups have a significant impact on the process of COLT, a large number of free radicals generated by the covalent bonds break from coal macromolecules during coal fragmentation, and the reaction of original functional groups can also participate in the COLT and has stronger reaction activity.[21] The COLT is a chain reaction process, which can be divided into chain initiation, chain propagation, and chain termination reactions.[4] In the chain initiation reaction stage, a large number of free radicals participate in a variety of reactions and release a large amount of heat, which is the key stage of the chain reaction.[4,53] Therefore, the active free radicals in the chain initiation stage were mainly considered in this paper, including alkyl free radicals ($\cdot CH_3$, R−$\cdot CH_2$), oxygen free radicals (R−O·), peroxy free radicals (R−OO·), and hydroxyl free radicals (·OH).

Since the coal macromolecular model is very complex, it is difficult to calculate the oxidation reaction process of each active group directly. According to previous studies, the properties of aromatic rings in coal molecules are very stable, and the chemical properties of active groups are not affected by aromatic rings.[54] Hence, the coal molecule can be simplified into small molecular fragments, that is, each small molecule is only composed of an active group and an aromatic ring. In this paper, the five active free-radical models contained in coal (·

https://doi.org/10.1021/acsomega.2c01229
ACS Omega 2022, 7, 18552−18568

CH_3, Ar−CH_2−·CH_2, Ar−CH_2−O·, Ar−CH_2−OO·, and ·OH) were constructed. Due to the active phenolic hydroxyl in BHT, it can capture active free radicals in coal as an electron or hydrogen donor and convert them into relatively stable compounds. After losing the H atom, BHT can form a ketone compound with stable properties, so as to terminate the chain reaction of free radicals and reduce the oxidation rate.[55] Therefore, the reaction pathways can be predicted, as shown in reactions 1−5.

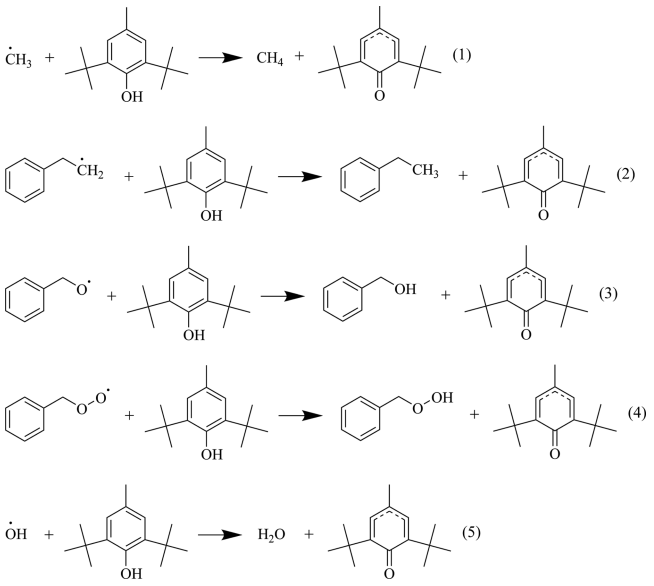

2.2.2. Molecular Structure Optimization. DFT is a common quantum chemical calculation method, which has the advantages of small calculated amounts and high precision. Therefore, it can be used to calculate the energy and electronic structure of the target system.[56] The B3LYP method in DFT was used to describe the electron exchange and correlation functional. The 6-311G (d, p) basis set was selected, and dispersion correction was carried out by using the Becke-Johnson damping function and Grimme's DFT-D3 algorithm.[57] The keywords were "Opt = Calcfc, B3LYP/6-311G (d, p), em = gd3". In addition, the ground state method was applied to optimize all molecules. The natural bond orbital was used to analyze the molecular orbital distribution and charges delocalization. It should be noted that the spin multiplicity is the difference between the number of α electrons and β electrons plus 1, and when the spin multiplicity is greater than 1, the calculation was carried out in the unrestricted system.

2.2.3. Surface Electrostatic Potential Analysis. The quantitative analysis of molecular surface is of great significance for predicting the reactive sites, binding modes, and thermodynamic properties of molecules. Surface electrostatic potential (ESP) is an index describing the interaction energy of charges in a molecular system at a certain point, and its expression is shown in formula 6.[58] In this paper, the van der Waals distribution of molecular ESP was used to predict the electrophilic and nucleophilic reaction centers of molecules. The regions with extremely positive (negative) ESP are more likely to attract nucleophilic (electrophilic) reagents for further reactions.

$$V_{tot}(r) = V_{nuc}(r) + V_{ele}(r) = \sum_A \frac{Z_A}{|r - R_A|} - \int \frac{\rho(r')}{|r - r'|} dr' \quad (6)$$

where R_A is the nucleus coordinates of atom A, Z_A represents the nuclear charges, and $\rho(r)$ is the electron density.

2.2.4. Transition-State Search and Intrinsic Reaction Coordinate (IRC) Analysis. According to the molecular characteristics of reactants and products, the TS (Berny, QST2) method was selected to search the transition state, whose keywords were "Opt = (Calcfc, ts, noeigen), 6-311G(d,p), em = gd3." The reaction pathway was verified by IRC,[27] and the local quadratic approximation (LQA) algorithm was used to track 20 points in the product and reactant directions in stepsize of 0.05 Bohr/s, and the Hessian matrix was accurately calculated every five steps, while other parameters remain the default. The keywords were "IRC = (Calcfc, maxpoints = 20, recalc = 5, stepsize = 10, LQA), B3LYP/6-311G(d,p), em = gd3." In addition, the vibration frequencies of reactant, transition state, and product of each reaction were calculated.

2.2.5. Calculation of Thermodynamic Parameters. Enthalpy (H) and Gibbs free energy (G) are important parameters to characterize the reaction activity of substances in thermodynamics. The enthalpy change (ΔH) is the difference of H between the product and reactant, while activation energy (ΔE) can be defined as the difference of G between transition state and reactant, that is, the maximum energy barrier to be overcome.[59] For any reaction, when $\Delta H > 0$, it indicates that the reaction is endothermic, and when $\Delta H < 0$, the reaction is exothermic. The smaller ΔE is, the easier the reaction is and the faster the reaction rate is. Based on this theory, the thermodynamic parameters of the proposed reaction were calculated.

2.2.6. Calculation of the Reaction Rate. Transition state theory (TST) is often applied to calculate the reaction rate constant of simple systems. It assumes that the reactants are in thermodynamic equilibrium due to the rapid energy exchange with the environment, and all reactants in the transition state can be converted into products.[47] The calculation formula is shown in formula 7.

$$k^{TST} = \sigma \frac{k_B T}{h} \left(\frac{RT}{P_0}\right)^{\Delta n} e^{-\Delta G^{0,\neq}/(k_B T)} \quad (7)$$

where $\sigma = 1$ is the degeneracy of the reaction pathway; $k_B = 1.381 \times 10^{-23}$ J/K is the Boltzmann constant; T is the ambient temperature; $h = 6.626 \times 10^{-34}$ J·s is the Planck constant; $R = 8.314$ J/(mol·K) is the universal constant; and $\Delta n = n - 1$ since the reaction is bimolecular, the value is set to 1; $P_0 = 101.325$ kPa is the standard state pressure, and $\Delta G^{0,\neq}$ is the activation energy of the standard state.

3. RESULTS AND DISCUSSION

3.1. Micromorphology Analysis. The micromorphology analysis can obtain the change in BHT on lignite physical properties. The results of Figure 2 show that the external outline of raw coal particles is clear with obvious lamellar structures. After the BHT is added, a large number of small particles are attached to the surface of the coal particles, and the outline is fuzzy. This is because BHT small particles can block the internal pores and cracks of coal particles, reduce the

https://doi.org/10.1021/acsomega.2c01229
ACS Omega 2022, 7, 18552−18568

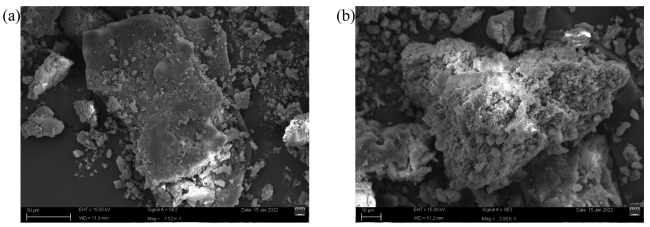

Figure 2. Micromorphology analysis of (a) raw coal and (b) BHT-Coal samples.

internal oxygen diffusion, and hinder the COLT to a certain extent.

3.2. In Situ FTIR Analysis. The in situ FTIR spectra of the raw data after smoothing is shown in Figure 3. It can be found that the spectra curves of raw coal and BHT-coal show obvious differences at the same temperature. At the same time, the spectra curves of the same sample also change significantly with the temperature rise.

In order to quantitatively analyze the variation law of active groups in the sample with temperature rise, the baseline correction of relevant test data was carried out using the peak fitting method. At the same time, the ratio of the area occupied by each peak to the total peak area was used as its content to eliminate the impact of baseline drift on the test results. The vibrations of $-CH_3$, $-CH_2$, and $-CH$ are in the wavenumber range of 2800−3000 cm^{-1}, and the vibration of $-OH$ is in the wavenumber range of 3000−3800 cm^{-1}. Furthermore, the vibration in the wavenumber range of 1000−1800 cm^{-1} belongs to oxygen-containing functional groups, which can be divided into the vibration of the C−O bond in the wavenumber range of 1000−1550 cm^{-1} and the vibration of C═O bond in the wavenumber range of 1550−1800 cm^{-1}.[60] The evolution law of each active group during COLT is shown in Figure 4.

Figure 4a shows the variation law of alkyl groups with temperature rise in raw coal and BHT-Coal. The alkyl groups mainly include $-CH_3$, $-CH_2$, and $-CH$, where the latter two have strong activity in the early stage of COLT. They can react with O_2 to form peroxy free radicals, which are the main exothermic reaction in the chain initiation stage and can provide heat for subsequent reactions. The results indicate that the alkyl groups in both samples gradually decrease with the increase in temperature, but the content of BHT-Coal is higher. This is because BHT can provide H atoms and react with peroxy free radicals to generate alkyl groups again, which hinders the progress of chain reactions.

Figure 4b shows the variation law of alkoxy groups with the temperature rise in raw coal and BHT-Coal. It can be seen that alkoxy groups in raw coal increase first and then decrease with the increase in temperature. The main reason is that the alkoxy groups can be oxidized by O_2 to form alkoxy groups during the COLT, and when the temperature is high enough, the alkoxy groups can continue to be oxidized to form carbonyl groups. The alkoxy groups in BHT-Coal gradually decrease with the increase in temperature. The main reason is that the addition of BHT reduces the contents of $-CH_2$ and $-CH$, which hinders the formation of alkoxy groups and reflects the inhibition effect of BHT.

Figure 4c shows the variation law of carbonyl groups with temperature rise in raw coal and BHT-Coal. Carbonyl groups mainly exist in aldehyde groups, carboxyl groups, and anhydrides. Aldehyde groups and carboxyl groups are the main sources of CO and CO_2 in the process of COLT, respectively, while the self-reactions between free radicals can generate secondary carbonyl groups. It can be seen from the results that the carbonyl groups in raw coal increase gradually with the increase in temperature, indicating that the formation rate of carbonyl is greater than the consumption rate. While in BHT-Coal, the carbonyl groups decrease gradually with the temperature rise, which is because the reactants that generate secondary carbonyl groups are reduced, hindering the chain reactions of COLT.

Figure 4d shows the variation law of hydroxyl groups with temperature rise in raw coal and BHT-Coal, and hydroxyl groups can be divided into free and associated. It can be seen from the results that the content of hydroxyl groups in raw coal gradually decreases with the increase in temperature, mainly because the hydroxyl groups can react with H atoms to generate H_2O or continue to participate in other oxidation reactions to consume. At 30 °C, the hydroxyl groups content of BHT-Coal is significantly higher than that of raw coal, which is because BHT is an antioxidant containing a large number of active phenolic hydroxyl groups, and the reaction rate is slow at

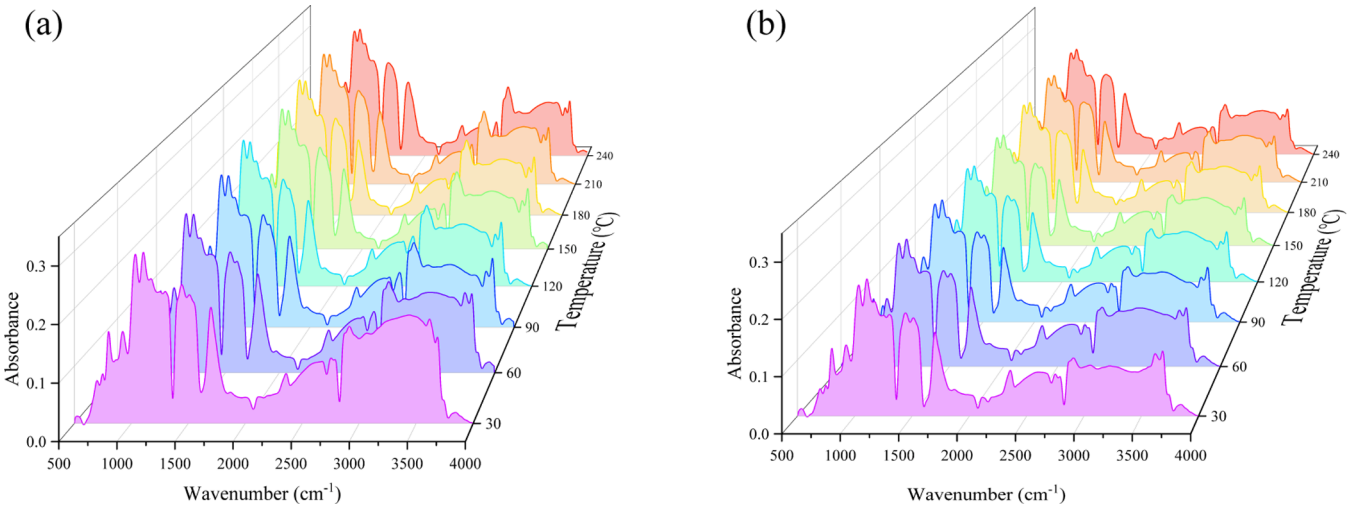

Figure 3. In situ FTIR spectra of (a) raw coal and (b) BHT-Coal.

https://doi.org/10.1021/acsomega.2c01229
ACS Omega 2022, 7, 18552−18568

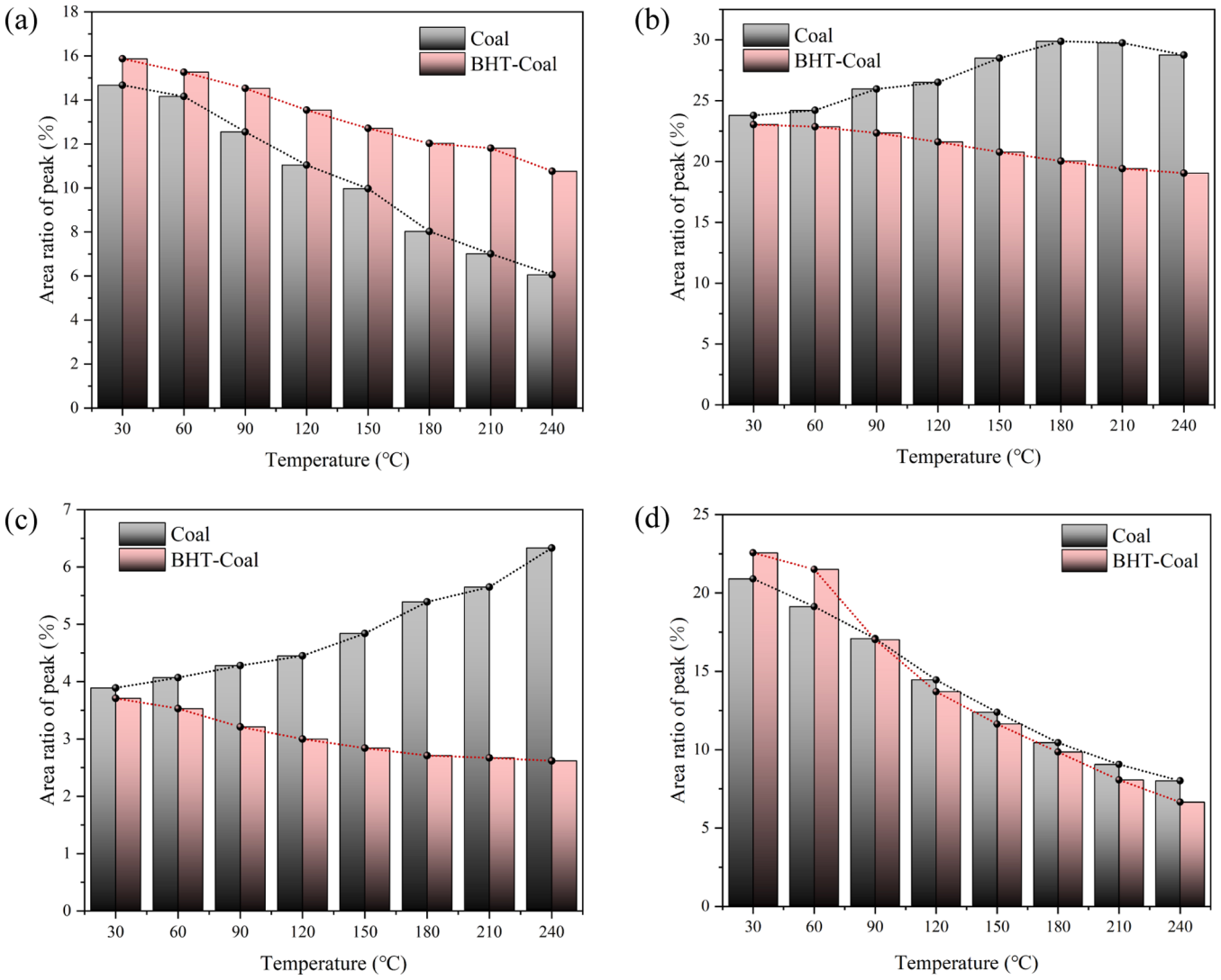

Figure 4. Content of (a) alkyl groups, (b) alkoxy groups, (c) carbonyl groups, and (d) hydroxyl groups at different temperatures in raw and BHT-Coal.

low temperature. With the increase in temperature, the active H atoms rapidly consume the free hydroxyl groups, so that the final content is lower than that of raw coal.

3.3. EPR Analysis. Figure 5 shows the EPR spectra of raw coal and BHT-Coal at 40, 60, 90, and 120 °C, respectively. From a macro point of view, all curves are basically the same, including a peak and a trough, without hyperfine structures. The spectra change trend in the same sample at different temperatures is basically the same, but the spectra before and after inhibition at the same temperature change obviously, indicating that the addition of BHT has a great impact.

Figure 6 shows the variation trend of the free-radical concentration (Ng), g value, and line width (ΔL) of raw coal and BHT-Coal with temperature rise.

Figure 6a shows the change law of Ng, that is, the content of the paramagnetic center in the test samples. It can be seen that the Ng of raw coal gradually increases with the temperature rise and is distributed between 3 and 5.5 × 10^{16}/g. The main reason is that the active groups (mainly alkyl groups) in coal react with O_2 to generate a large number of free radicals, which leads to the chain reactions of free radicals. With the increase in temperature, more heat can be obtained in the reaction process, and the free-radical reactions are more intense. However, the Ng of BHT-Coal does not increase with the temperature rise and even shows a slight downward trend, indicating that BHT is effective in reducing the concentration of free radicals in coal.

Figure 6b shows the variation curve of g with temperature rise, which is very sensitive to the chemical environment and can reflect the position of unpaired electrons in paramagnetic molecules. The g is related to the types of free radicals. At room temperature and pressure, the g of lignite is higher than that of free electrons (g_e = 2.0023), which is related to the coupling of spin orbits.[43] It can be seen from the results that the g of raw coal gradually increases with the temperature rise, mainly because the formation of chain reactions greatly increases the types of free radicals. At the same temperature, the g of BHT-Coal is less than that of raw coal and decreases with the increase in temperature, indicating that BHT can reduce the types and content of free radicals.

Figure 6c shows change law of the ΔL with the temperature rise. The ΔL represents the interaction between free radicals and the microcrystalline structure of coal, namely, the energy exchange. Its calculation method is the difference between the

https://doi.org/10.1021/acsomega.2c01229
ACS Omega 2022, 7, 18552−18568

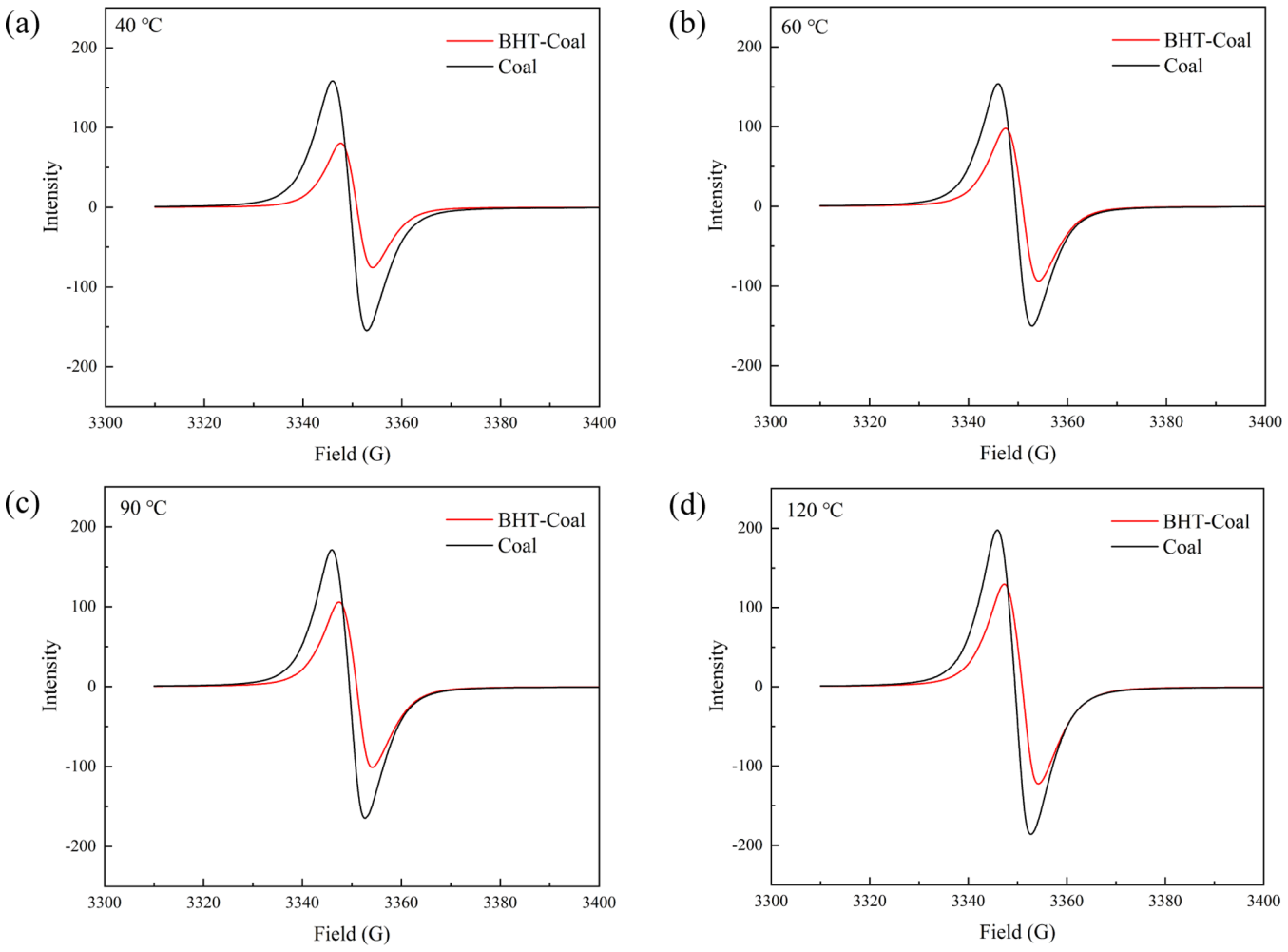

Figure 5. EPR spectra of raw coal and BHT-Coal at (a) 40, (b) 60, (c) 90, and (d) 120 °C.

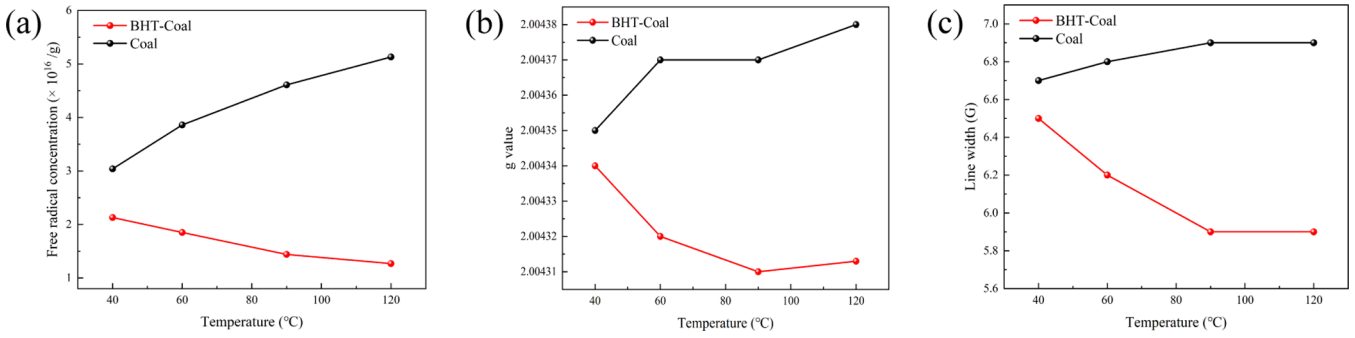

Figure 6. Variation trends of (a) Ng, (b) *g*, and (c) Δ*L* of raw coal and BHT-Coal with temperature rise.

abscissa of peak and trough of EPR spectrum. The results show that with the increase in temperature, the Δ*L* of raw coal gradually increases, which is mainly due to the chain reaction process greatly increases the content of free radicals, loosens the molecular structure, weakens the spin lattice effect, and shortens the relaxation time.

The EPR results show that BHT can reduce the content and types of free radicals in coal and then inhibit the chain reactions of the COLT.

3.4. Gas Production Experiments of COLT Analysis. The concentration variation curves of CO, CO_2, and C_2H_4 with the temperature rise are shown in Figure 7a–c, respectively.

It can be seen from the results that the concentrations of the three main gas products increase exponentially with the temperature rise. The raw coal begins to produce CO at 30 °C, while the BHT-Coal produces CO after 50 °C, and the concentration of the later is always lower than that of the former. The main reason for this phenomenon is that CO mainly comes from the dealdehyde reaction of aldehyde free radicals in the process of COLT,[28] and the H atoms of BHT can effectively hinder the formation of secondary aldehyde free radicals.

https://doi.org/10.1021/acsomega.2c01229
ACS Omega 2022, 7, 18552−18568

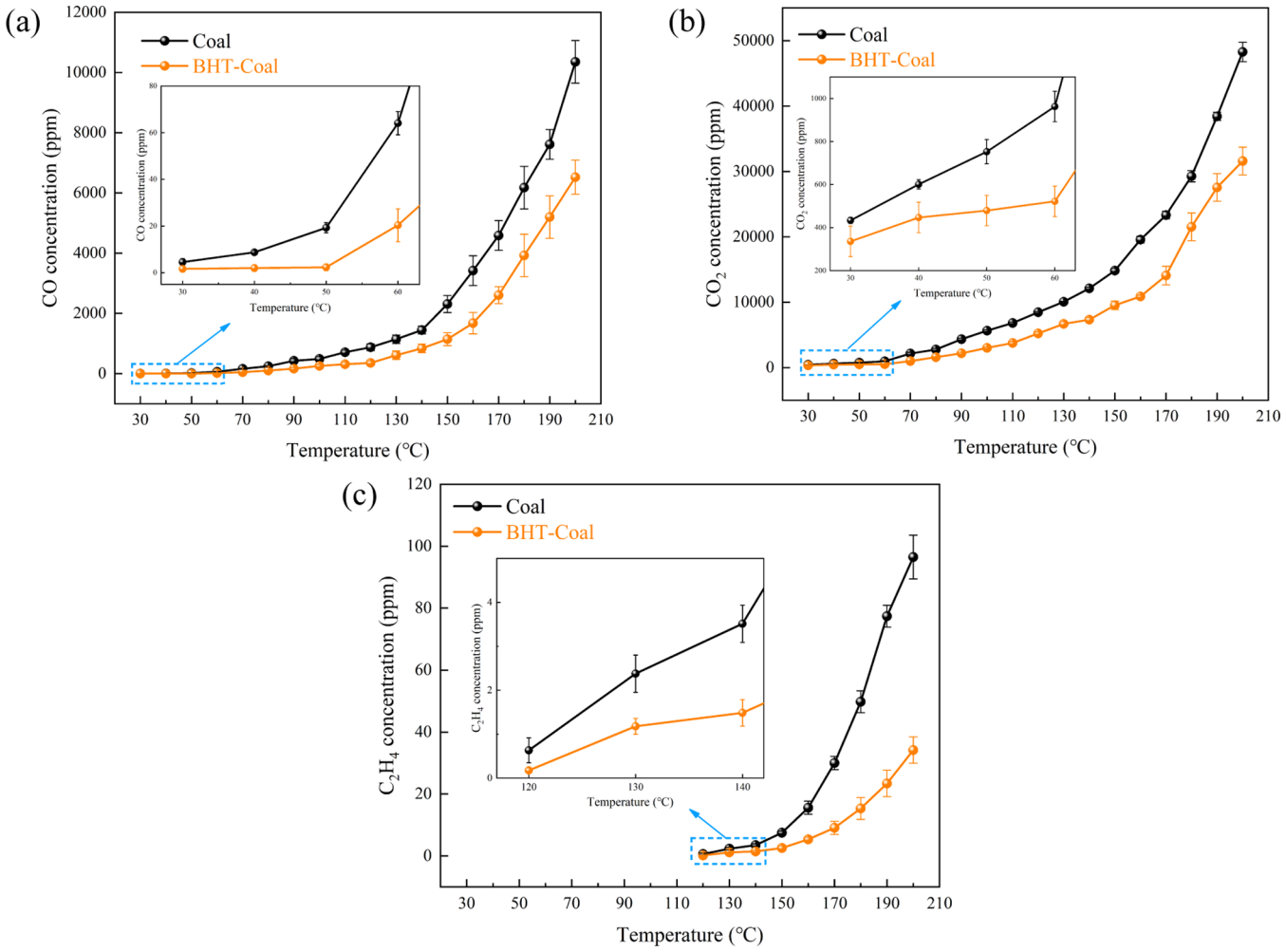

Figure 7. Variation curves of (a) CO, (b) CO_2, and (c) C_2H_4 concentration with temperature.

The variation trend of CO_2 is similar to that of CO, but the concentration is much higher. The source of CO_2 is mainly composed of two parts. A small amount of CO_2 generates before 50 °C, which comes from the desorption of CO_2 adsorbed by pores in coal. The amount of CO_2 increases greatly after 50 °C, coming from the decarboxylation of carboxyl free radicals.[28] The H atom of the phenolic hydroxyl group in BHT can also hinder the formation of secondary carboxyl free radicals, so that the CO_2 production concentration of BHT-Coal is lower than that of raw coal. The H atoms of BHT can also hinder the formation of secondary carboxyl free radicals, so that the CO_2 concentration of the BHT-Coal sample is lower than that of raw coal.

The formation law of C_2H_4 is the same as the first two, but the concentration is much less. There is no C_2H_4 formation before 120 °C, and the concentration of the BHT-Coal is always lower than that of raw coal. The main source of hydrocarbons in coal is the cracking and desorption of alkyl free radicals,[27] while the H atoms of BHT can reduce alkyl free radicals to alkyl groups, increasing the energy required for the formation of hydrocarbons.

Figure 8 shows the change in CPT. It can be seen from the results that the CPT of the raw coal is 132.3 °C, while that of the BHT-Coal is 157.4 °C, which is 25.1 °C higher than that of the former, indicating that BHT can inhibit the COLT to a certain extent.

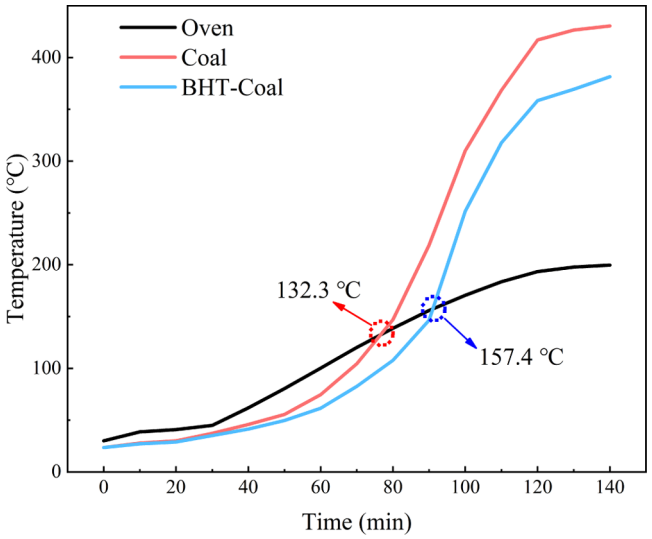

Figure 8. CPTs of raw coal and BHT-Coal.

3.5. Quantum Chemical Calculation and Analysis. *3.5.1. Molecular Structure Optimization and Reaction Activity Analysis.* Active sites are the most vulnerable reaction sites during the COLT.[61] In this paper, the geometric structure

https://doi.org/10.1021/acsomega.2c01229
ACS Omega 2022, 7, 18552−18568

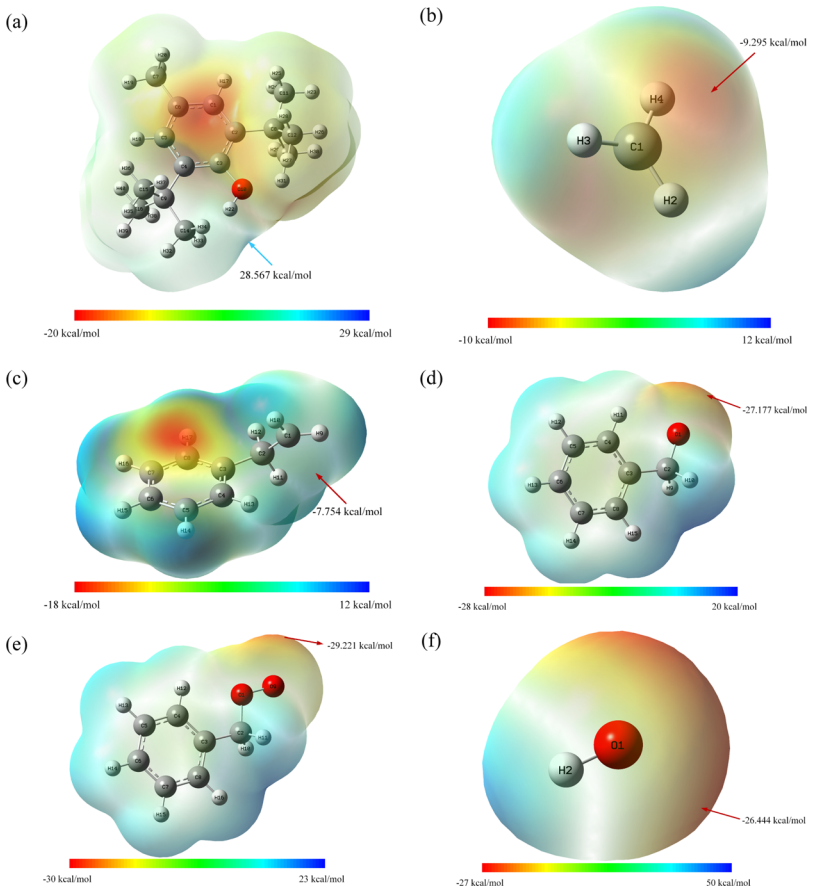

Figure 9. ESP isosurface maps of (a) BHT, (b) ·CH_3, (c) Ar−CH_2−·CH_2, (d) Ar−CH_2−O·, (e) Ar−CH_2−OO·, and (f) ·OH.

Table 2. Active Site and Its ESP Value of Each Molecule

categories	BHT	·CH_3	Ar−CH_2−·CH_2	Ar−CH_2−O	Ar−CH_2−OO·	·OH
atom	H22	C1	C1	O1	O9	O1
ESP	28.567	−9.295	−7.754	−27.177	−29.221	−26.444

and ESP of each active group were calculated by DFT, and the results are shown in Figure 9.

In general, the ESP of the blue region is positive, which is prone to the nucleophilic reaction, while that of the red region is negative, which is prone to the electrophilic reaction.[59] According to statistics, the ESP near the H atom of −OH in the BHT molecule is the maximum, which easily provides electrons and is a nucleophilic reagent. The minimum ESP of the five typical active groups is located near O or C atoms, which easily obtain electrons and are electrophilic reagents. The results show that the minimum ESP of ·CH_3, Ar−CH_2−O·, Ar−CH_2−OO·, and ·OH is located near the atoms, while that of Ar−CH_2−·CH_2 is located near the benzene ring. However, affected by the π−π* bond, the benzene ring structure is very stable and difficult to react; the second minimum is located near the C1 atom, which is the reaction-active site of Ar−CH_2−·CH_2. The extreme ESP values near the active site of each molecule are shown in Table 2.

3.5.2. Molecular Frontier Orbital Analysis. According to molecular frontier orbital theory, the occurrence of the chemical reaction is due to the mutual attraction between the highest occupied molecular orbital or single occupied molecular orbital (HOMO/SOMO) and the lowest unoccupied molecular orbital or SOMO (LUMO/SOMO) of the reactants. The electrons in the frontier orbitals are usually more active than the others, which easily cause electrons transfer, bond formation, or bond breaking and then leads to reactions taking place. Therefore, the bonding characteristics of the chemical reaction depend on the activity of electrons in the frontier orbitals.[62] As a nucleophilic reagent, BHT easily loses electrons, and the active bond is located on the largest electron cloud in HOMO. The active free radicals are electrophilic reagents, they easily obtain electrons, and the active bonds are located on the largest electron clouds on the SOMO. The results are shown in Figure 10.

The results show that the largest electron cloud on the HOMO of BHT molecule is located on the benzene ring. Because the chemical bonds of the benzene ring are relatively stable, they do not easily react, and the π bond orbital on the benzene ring can overlap laterally to form a closed conjugated large π bond, making the chemical properties more stable. Therefore, the reaction activity of the atoms on the benzene ring is lower than that of side-chain atoms, and the largest electron cloud is located on the O10−H22 bond. The largest electron cloud on SOMO of ·CH_3, Ar−CH_2−O·, Ar−CH_2−OO·, and ·OH is located on C1, C1, O1, O9, and O1 atoms, respectively, which can capture the H atom of phenolic

https://doi.org/10.1021/acsomega.2c01229
ACS Omega 2022, 7, 18552−18568

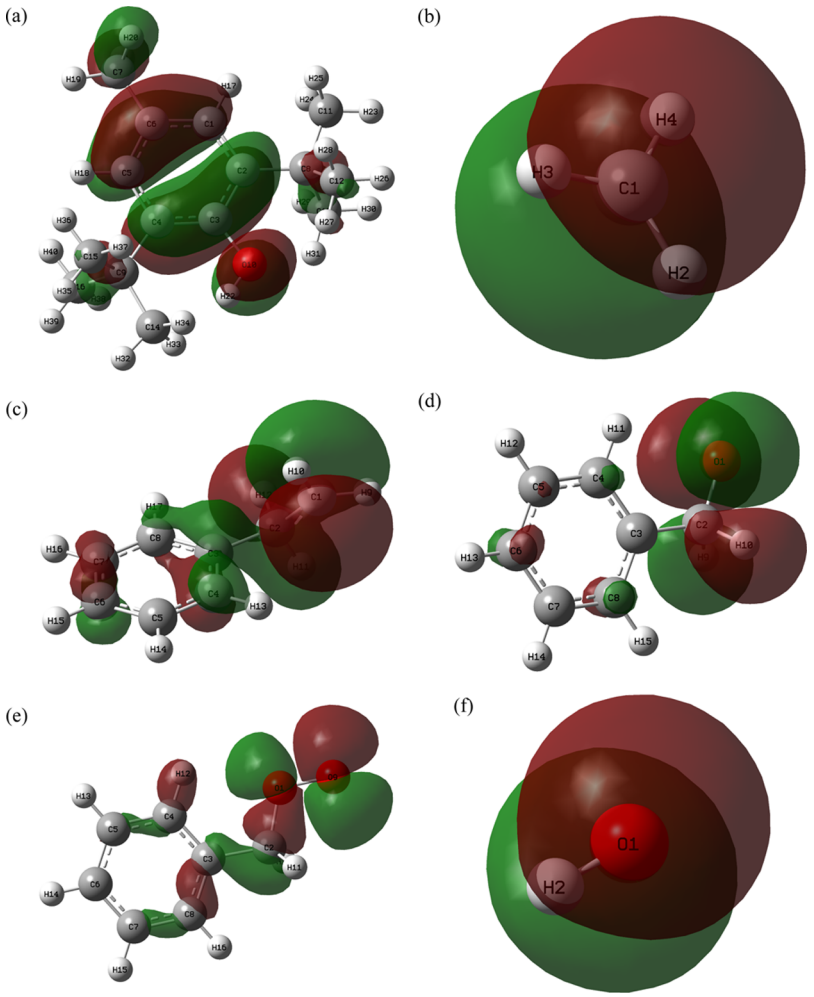

Figure 10. Electron cloud distribution in frontier molecular orbitals of (a) BHT, (b) ·CH_3, (c) Ar−CH_2−·CH_2, (d) Ar−CH_2−O·, (e) Ar−CH_2−OO·, and (f) ·OH.

hydroxyl in BHT to generate a substance with more stable properties. The results are the same as those of ESP analysis.

3.5.3. IRC and Thermodynamic Parameter Calculation. 3.5.3.1. Elementary Reaction between BHT and ·CH_3. The TS (Berny) method is applied for the transition-state search. Because there is an unpaired electron in the reactants, the spin multiplicity is set to 2, and it takes place in the unrestricted system. The calculation shows that the transition state has a unique virtual frequency of −1476.31, and the vibration direction corresponds to the reactant and product, which verifies the accuracy of the IRC. The change in total energy and the molecular structure of each stagnation point are shown in Figure 11.

The structure of each stagnation point is optimized, and the thermodynamic parameters are calculated, as shown in Table 3. The results indicate that the reaction pathway is correct and feasible. During the reaction, the O10−H44(Reactant, $R_{O10-H44}$ = 0.963 Å) bond is the active bond and breaks, which is consistent with the conclusion obtained from the molecular frontier orbital analysis above. After the O10−H44 bond breaks, the H44 atom moves away from the O10 atom to the C40 atom (transition state, $R_{O10-H44}$ = 1.098 Å) and finally forms the C40−H44 covalent bond (product, $R_{O10-H44}$ = 2.647 Å). After losing H44 atom, the BHT molecule forms a cyclohexenone compound. This structure is very stable and is not easily participate in the subsequent chain reactions. After ·CH_3 captures H44 atom, C40 atom changes from sp^2 to sp^3 hybridization, and the configuration changes from the original plane structure to the tetrahedral structure to form a CH_4 molecule, which will escape from the coal under the influence of high temperature. The reaction needs to overcome the reaction energy barrier of 33.147 kJ/mol and can release the heat of 133.604 kJ/mol, indicating that the reaction can be carried out at room temperature or higher.

3.5.3.2. Elementary Reaction between BHT and Ar−CH_2−·CH_2. Using the same method to search for the transition state, it can be seen that there is a unique virtual frequency of −1796.31. The positive end of the IRC curve corresponds to the product, and the reverse end corresponds to the reactant. Both of them have no virtual frequency, which verifies the correctness of the reaction pathways. The change in total energy and the molecular structure of each stagnation point are shown in Figure 12.

The structure of each stagnation point is optimized, and the thermodynamic parameters are calculated, as shown in Table 4. The reaction mechanism of BHT molecule is the same as that of reaction 1. The equilibrium distance of O10−H22 gradually increases from 0.963 Å to 2.547 Å during the reaction process. At the same time, the equilibrium distance of C41−H22 gradually shortens. After obtaining the H22 atom,

https://doi.org/10.1021/acsomega.2c01229
ACS Omega 2022, 7, 18552−18568

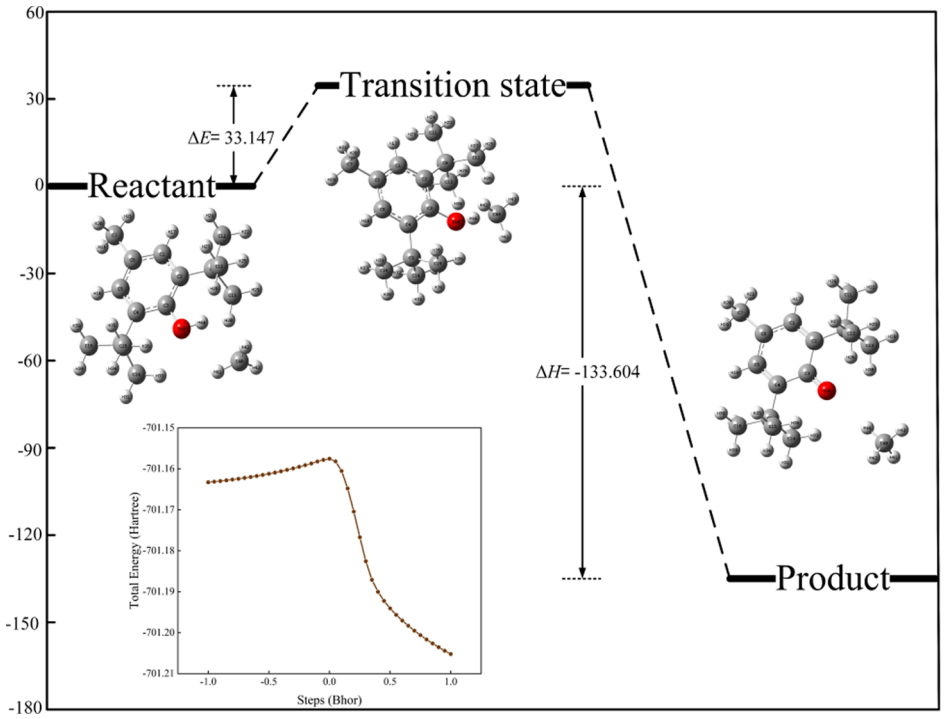

Figure 11. Total energy change and molecular structure of each stagnation point in reaction 1.

Table 3. Thermodynamic Parameters of Reaction 1[a]

categories	enthalpy H (Hartree)	Gibbs free energy G (Hartree)	enthalpy change ΔH (kJ/mol)	activation energy ΔE (kJ/mol)	reaction rate k ($cm^3/mol/s$)
reactant	−700.753567	−700.833378	−133.604	33.147	3.987×10^{-13}
transition state	−700.7496	−700.820753			
product	−700.804454	−700.886805			

[a]Note that 1 Hartree = 627.51 kcal/mol = 2625.5 kJ/mol.

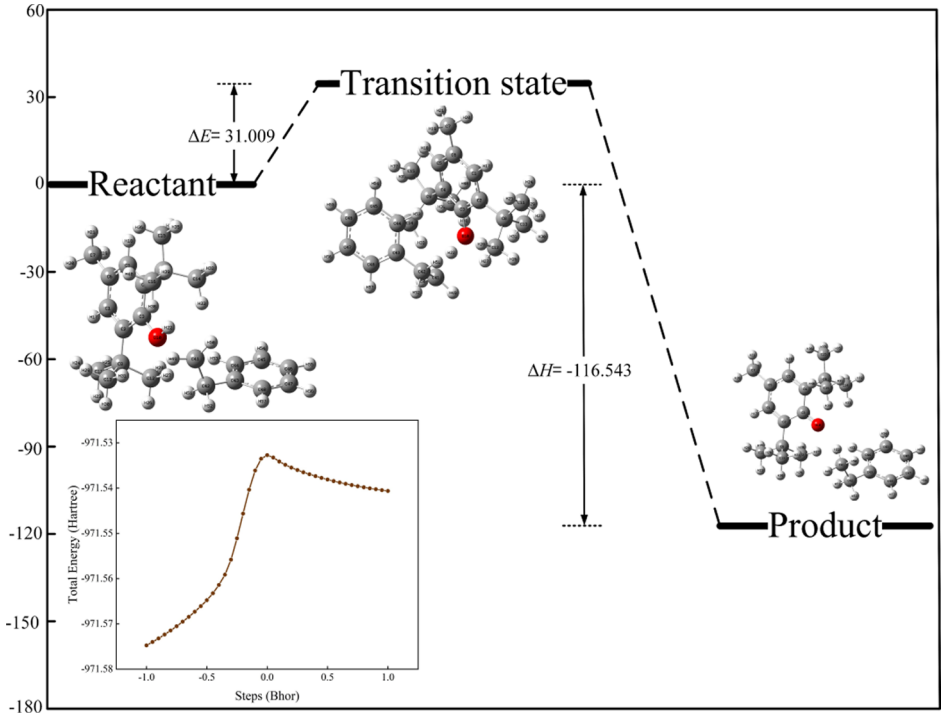

Figure 12. Total energy change and molecular structure of each stagnation point in reaction 2.

https://doi.org/10.1021/acsomega.2c01229
ACS Omega 2022, 7, 18552−18568

Table 4. Thermodynamic Parameters of Reaction 2[a]

categories	enthalpy H (Hartree)	Gibbs free energy G (Hartree)	enthalpy change ΔH (kJ/mol)	activation energy ΔE (kJ/mol)	reaction rate k (cm^3/mol/s)
reactant	−971.016297	−971.104589	−116.543	31.009	9.446×10^{-13}
transition state	−971.008443	−971.092778			
product	−971.060686	−971.15217			

[a]Note that 1 Hartree = 627.51 kcal/mol = 2625.5 kJ/mol.

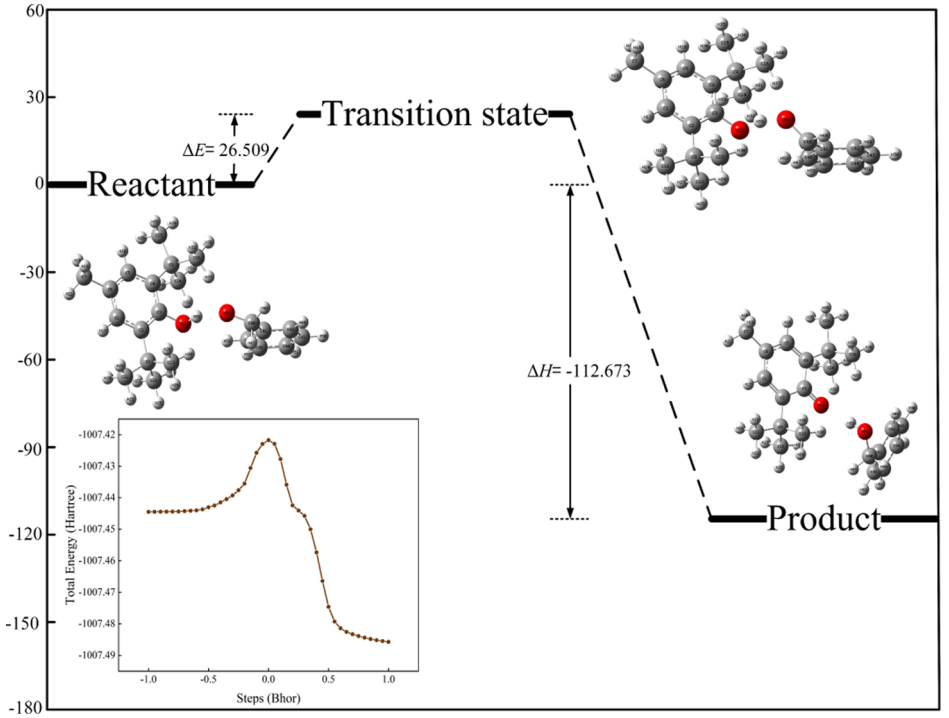

Figure 13. Total energy change and molecular structure of each stagnation point in reaction 3.

Table 5. Thermodynamic Parameters of Reaction 3[a]

categories	enthalpy H (Hartree)	Gibbs free energy G (Hartree)	enthalpy change ΔH (kJ/mol)	activation energy ΔE (kJ/mol)	reaction rate k (cm^3/mol/s)
reactant	−1006.940054	−1007.029897	−112.673	26.509	5.802×10^{-12}
transition state	−1006.915395	−1007.0198			
product	−1006.982969	−1007.073479			

[a]Note that 1 Hartree = 627.51 kcal/mol = 2625.5 kJ/mol.

the C41 atom changes from sp^2 to sp^3 hybrid, and C41 forms a σ bond by s-sp^3 hybridization with the H22 atom, where the bond length is 1.098 Å. The angle of H50−C41−H49 in Ar−CH_2−·CH_2 twists from 117.854 to 109.466°, and the angle between the C24−C22 bond and H30−C24−H31 plane twists from the plane structure to 122.058°. The micro parameters of the product are consistent with those of −CH_3, indicating that the H22 atom has completely separated from the phenolic hydroxyl structure to reach a stable state. The reaction needs to overcome the energy barrier of 31.009 kJ/mol and release the heat of 1116.543 kJ/mol, indicating that the reaction can take place at room temperature or higher.

3.5.3.3. Elementary Reaction between BHT and Ar−CH_2−O·. The transition state has a unique virtual frequency of −933.07, and both the transition state and IRC are verified as correct. The change in total energy and the molecular structure of each stagnation point are shown in Figure 13.

The thermodynamic parameters of reaction 3 are shown in Table 5. After the O10−H55 bond breaks, the H55 atom moves toward the O54 atom, the equilibrium distance between O54 and H55 shortens from 1.927 to 0.973 Å, and a covalent bond forms. At the same time, the bond angle of C40−O54−H55 gradually twists from 153.76 to 107.99°. During the reaction, the energy barrier of 26.509 kJ/mol needs to be overcome, and a total of 112.673 kJ/mol of heat is released. The energy required for the reaction is very low and can occur at room temperature and pressure.

3.5.3.4. Elementary Reaction between BHT and Ar−CH_2−OO·. The transition state has a unique virtual frequency of −1433.18, and both the transition state and IRC are verified as correct. The change in total energy and the molecular structure of each stagnation point are shown in Figure 14.

The structure of each stagnation point is optimized, and the thermodynamic parameters are calculated, as shown in Table 6. After the O10−H22 bond breaks, H22 is attracted by the charge carried by Ar−CH_2−OO·, and the distance between H22 and O56 shortens from 1.946 to 0.979 Å to form a hydroperoxide. It is worth noting that Ar−CH_2−OOH is not

https://doi.org/10.1021/acsomega.2c01229
ACS Omega 2022, 7, 18552−18568

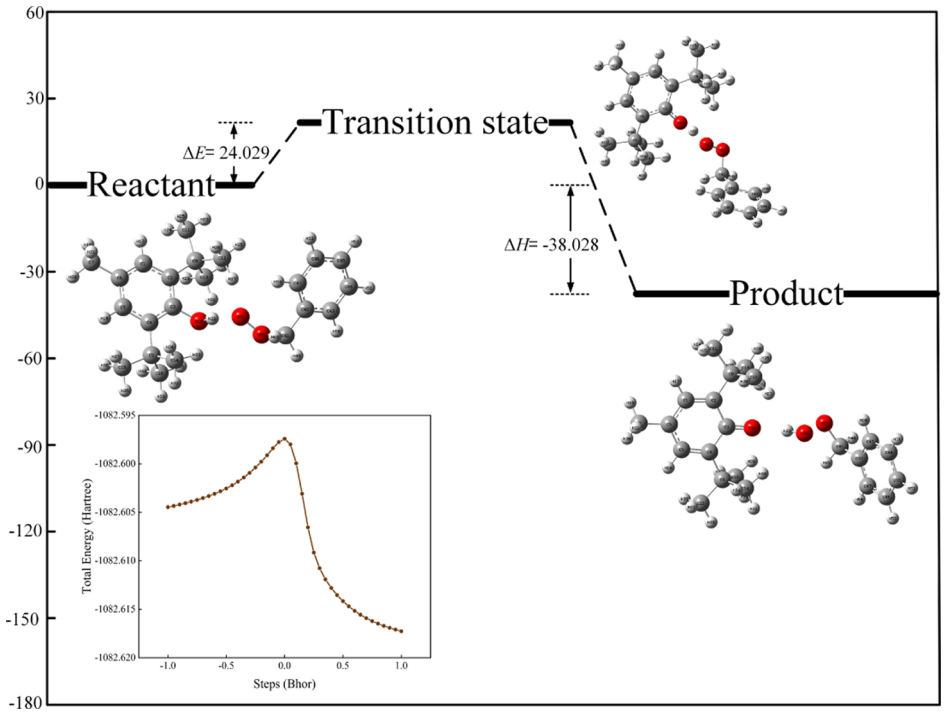

Figure 14. Total energy change and molecular structure of each stagnation point in reaction 4.

Table 6. Thermodynamic Parameters of Reaction 4[a]

categories	enthalpy H (Hartree)	Gibbs free energy G (Hartree)	enthalpy change ΔH (kJ/mol)	activation energy ΔE (kJ/mol)	reaction rate k (cm^3/mol/s)
reactant	−1082.095464	−1082.189928	−38.028	24.029	1.587×10^{-11}
transition state	−1082.090862	−1082.180776			
product	−1082.109948	−1082.203329			

[a]Note that 1 Hartree = 627.51 kcal/mol = 2625.5 kJ/mol.

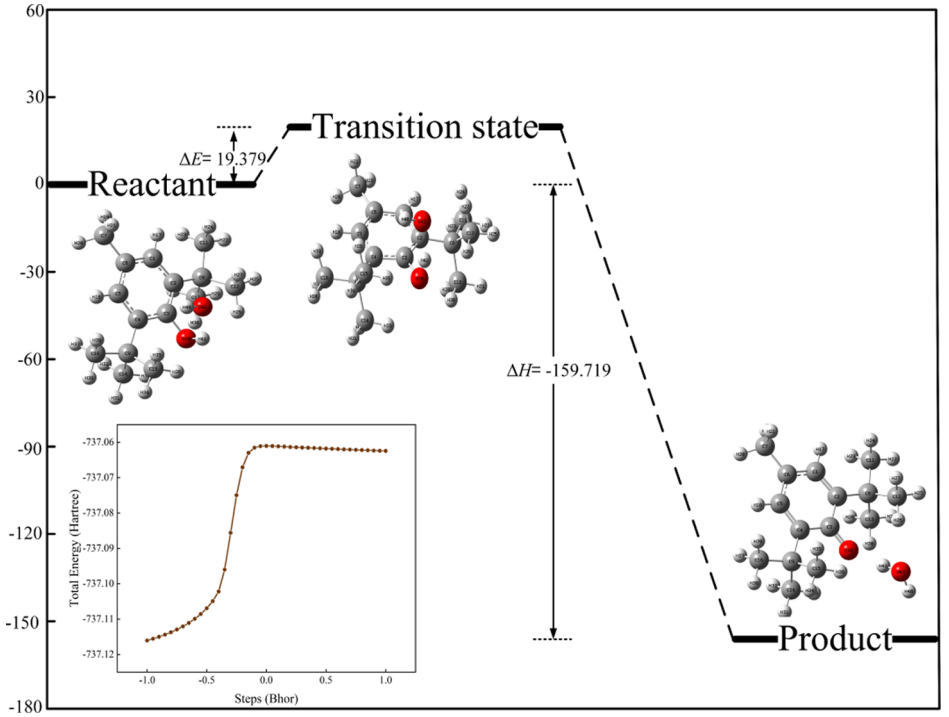

Figure 15. Total energy change and molecular structure of each stagnation point in reaction 5.

https://doi.org/10.1021/acsomega.2c01229
ACS Omega 2022, 7, 18552−18568

Table 7. Thermodynamic Parameters of Reaction 5[a]

categories	enthalpy H (Hartree)	Gibbs free energy G (Hartree)	enthalpy change ΔH (kJ/mol)	activation energy ΔE (kJ/mol)	reaction rate k (cm^3/mol/s)
reactant	−736.672128	−736.742122	−159.719	19.379	1.030×10^{-10}
transition state	−736.673119	−736.734741			
product	−736.732962	−736.805792			

[a]Note that 1 Hartree = 627.51 kcal/mol = 2625.5 kJ/mol.

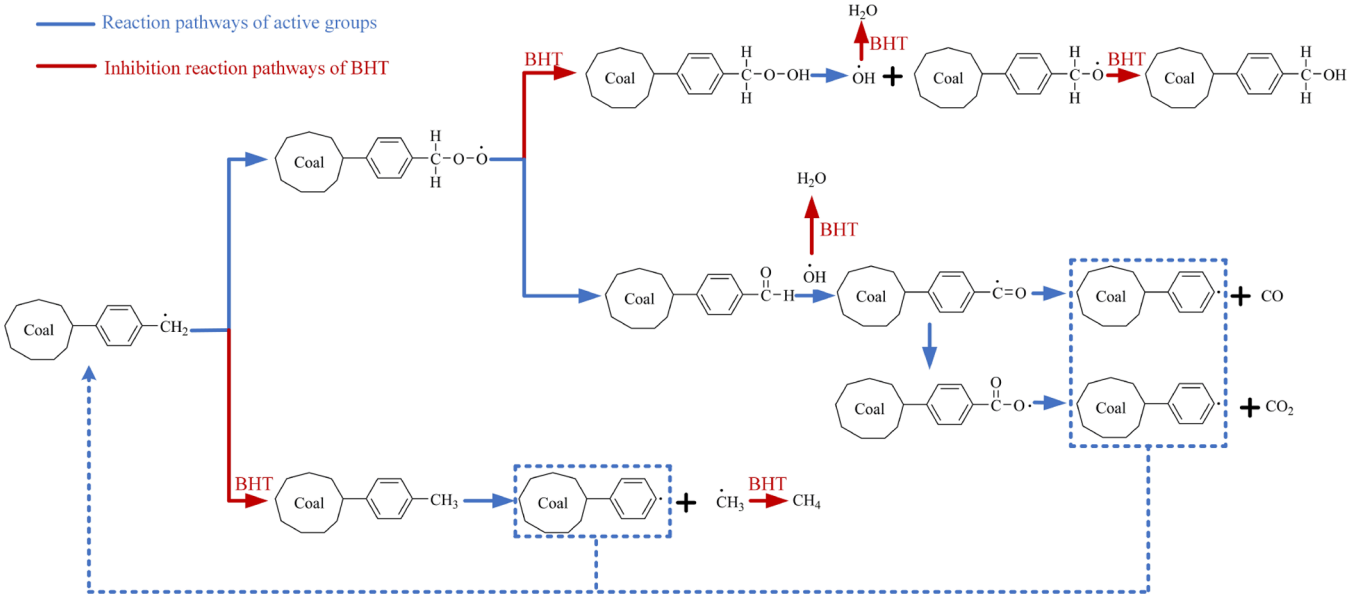

Figure 16. Inhibition mechanism and process of BHT on the chain reaction of COLT.

stable. In the subsequent reaction, the O55−O56 bond increases from 1.384 to 1.458 Å, indicating that the bond can break under the action of heat to form an oxygen free radical and a hydroxyl free radical. The products are both active free radicals and can continue to be oxidized by BHT to form stable compounds. The whole reaction needs to overcome the energy barrier of 24.029 kJ/mol, which shows that the reaction can take place spontaneously at room temperature, reflecting the effectiveness of BHT as an antioxidant. The heat release is −38.028 kJ/mol, which has a certain thermal effect.

3.5.3.5. Elementary Reaction between BHT and ·OH. The transition state has a unique virtual frequency of −359.93, and both the transition state and IRC are verified as correct. The change in total energy and the molecular structure of each stagnation point are shown in Figure 15.

The structure of each stagnation point is optimized, and the thermodynamic parameters are calculated, as shown in Table 7. The equilibrium distance of O10−H41 increases gradually, indicating that the covalent bond breaks, and H41 atom has separated from the adsorption of O10 atom. Compared with the reactant and transition state, the O42−H41 bond of the product further shortens, while the O42−O21 bond remains basically unchanged, the length is stable at 0.973 Å, and the bond angle of H41−O42−H40 gradually increases from 122.37 to 104.48°, which is basically consistent with the empirical value of the H_2O molecular structure, indicating that H_2O molecule has completely formed an independent and stable structure. At this time, the 2s, 2px, 2py, and 2pz orbitals of the O42 atom are all sp^3 hybridized, in which two orbitals are occupied by two lone pairs electrons, and the other two form σ bond with H19 and H21. Since the hybrid orbital electron cloud occupied by the lone pair electrons is denser, the hybrid orbital occupied by the bonding electron pair is repelled and compressed, so that the angle between the two O−H bonds is compressed to 104.48°, which forms a V-shaped structure. The activation energy required for this reaction is very small (ΔE = 19.379 kJ/mol), and the heat release (ΔH) is −159.719 kJ/mol, which is an exothermic reaction. The results show that the reaction can occur spontaneously at room temperature and pressure, reflecting the universality of BHT as an antioxidant.

4. INHIBITION MECHANISM OF BHT ON THE COLT

It can be seen from the above analyses that BHT, as a H atom donor, can quickly react with the active free radicals in coal at room temperature and pressure, and the H atom can pair with the lone pair electrons with high activity and lose the reaction activity. The ΔE order of BHT reacting with the five active radicals is ·CH_3 > Ar−CH_2−·CH_2 > Ar−CH_2−O· > Ar−CH_2−OO· > ·OH, and the order of the reaction rate is just the opposite. Therefore, in the BHT inhibition process, it preferentially reacts with ·OH and peroxy free radicals, while the reaction ability with alkyl free radicals is weak, which is consistent with the research results that ·OH has the strongest reaction activity.[21] The results show that the main way for BHT inhibiting the coal spontaneous combustion is to consume highly active ·OH and peroxy free radicals during the COLT to form stable compounds and control the reaction rate of active free radicals. The specific inhibition mechanism and process are shown in Figure 16.

https://doi.org/10.1021/acsomega.2c01229
ACS Omega 2022, 7, 18552−18568

Overall, the inhibition characteristic of BHT is to cut off the chain reactions of active free radicals, greatly reduce the concentration and activity of them, so as to slow down the reaction rate. From a macro point of view, BHT can reduce the release concentration of index gas during the COLT and increase the CPT. At the micro level, the contents of active free radicals and functional groups in coal samples are changed.

5. CONCLUSIONS

In this paper, the characteristics of BHT inhibiting the COLT are studied by means of experiments and quantum chemical calculations. The main conclusions are as follows:

(1) The results of in situ FTIR show that the active groups of BHT-Coal change weakly when the temperature is lower than 40 °C but decrease significantly with the increase in temperature. It is worth noting that the content of alkyl groups in the BHT-Coal is always higher than that of raw coal, while others (alkoxy, carbonyl, and hydroxyl) are lower than that of raw coal, indicating that BHT can block the chemical oxygen absorption reactions of alkyl groups and reduce the formation of alkyl free radicals.

(2) EPR analysis shows that the Ng, g, and ΔL of active free radicals in raw coal increase with the temperature rise, while the three of the BHT-Coal decrease, indicating that BHT can effectively reduce the types and contents of active radicals during the COLT.

(3) The results of gas production experiments show that compared with raw coal, the production temperature of CO, CO_2, and C_2H_4 of BHT-Coal is raised, and the concentration is also reduced. The CPT increases from 132.3 to 157.4 °C, indicating that BHT can effectively reduce the rate of COLT.

(4) In order to better explore the inhibition mechanism and process of BHT, the molecular models of BHT and five typical active free radicals are established. The ESP, molecular frontier orbital, and inhibition pathways are explored at the micro level by the DFT, and the thermodynamic parameters of each reaction are calculated. The results show that the H atoms of the phenolic hydroxyl groups in BHT can be captured by the active free radicals to form stable compounds, then the BHT molecules are transformed into stable cyclohexenone compound. At the same time, the ΔE of each reaction is very small and can occur at room temperature and pressure, indicating that the inhibition mechanism of BHT is to make the active free radicals in coal lose the reaction activity and reduce the concentration, so as to cut off the chain reactions of the COLT.

AUTHOR INFORMATION

Corresponding Author

Hongqing Zhu − *School of Emergency Management and Safety Engineering, China University of Mining and Technology (Beijing), Beijing 100083, China*; Phone: 13700131805; Email: zhqcumtb1@163.com

Authors

Yujia Huo − *School of Emergency Management and Safety Engineering, China University of Mining and Technology (Beijing), Beijing 100083, China*; orcid.org/0000-0001-9432-6164

Xin He − *School of Emergency Management and Safety Engineering, China University of Mining and Technology (Beijing), Beijing 100083, China*; orcid.org/0000-0003-1677-5954

Complete contact information is available at: https://pubs.acs.org/10.1021/acsomega.2c01229

Author Contributions

H.Z. wrote review and editing; Y.H. wrote original draft, experiments, simulation methods, and data arrangement; and X.H. completed the experimental test.

Notes

The authors declare no competing financial interest.

ACKNOWLEDGMENTS

This study was funded by the National Key R&D Program of China (grant no. 2016YFC0801800), the National Natural Science Foundation of China (grant nos. 51704299, 51804311, and 52074304), and the Open Research Fund of State Key Laboratory of Coal Mine Safety Technology (project no. sklcmst102).

REFERENCES

(1) Belviso, C. State-of-the-art applications of fly ash from coal and biomass: A focus on zeolite synthesis processes and issues. *Prog. Energy Combust. Sci.* **2018**, *65*, 109−135.

(2) Zhang, J.; Ren, T.; Liang, Y.; Wang, Z. A review on numerical solutions to self-heating of coal stockpile: Mechanism, theoretical basis, and variable study. *Fuel* **2016**, *182*, 80−109.

(3) Huo, Y.; Zhu, H.; He, X.; Fang, S.; Wang, W. Quantum Chemical Calculation of the Effects of H2O on Oxygen Functional Groups during Coal Spontaneous Combustion. *ACS Omega* **2021**, *6*, 25594−25607.

(4) Huo, Y.; Zhu, H.; He, X.; Fang, S.; Wang, W. Quantum Chemistry Calculation Study on Chain Reaction Mechanisms and Thermodynamic Characteristics of Coal Spontaneous Combustion at Low Temperatures. *ACS Omega* **2021**, *6*, 30841−30855.

(5) Song, Z.; Kuenzer, C. Coal fires in China over the last decade: A comprehensive review. *Int. J. Coal Geol.* **2014**, *133*, 72−99.

(6) Atalay, F.; Tercan, A. E. Coal resource estimation using Gaussian copula. *Int. J. Coal Geol.* **2017**, *175*, 1−9.

(7) Nimaje, D. S.; Tripathy, D. P. Characterization of some Indian coals to assess their liability to spontaneous combustion. *Fuel* **2016**, *163*, 139−147.

(8) Lee, S.-S.; Wilcox, J. Behavior of mercury emitted from the combustion of coal and dried sewage sludge: The effect of unburned carbon, Cl, Cu and Fe. *Fuel* **2017**, *203*, 749−756.

(9) Rao, Z.; Zhao, Y.; Huang, C.; Duan, C.; He, J. Recent developments in drying and dewatering for low rank coals. *Prog. Energy Combust. Sci.* **2015**, *46*, 1−11.

(10) Wang, H.; Tan, B.; Shao, Z.; Guo, Y.; Zhang, Z.; Xu, C. Influence of different content of FeS2 on spontaneous combustion characteristics of coal. *Fuel* **2021**, *288*, 119582.

(11) Wang, H.; Dlugogorski, B. Z.; Kennedy, E. M. Coal oxidation at low temperatures: oxygen consumption, oxidation products, reaction mechanism and kinetic modelling. *Prog. Energy Combust. Sci.* **2003**, *29*, 487−513.

(12) Xin, H.-h.; Wang, D.-m.; Dou, G.-l.; Qi, X.-y.; Xu, T.; Qi, G.-s. The Infrared Characterization and Mechanism of Oxygen Adsorption in Coal. *Spectrosc. Lett.* **2014**, *47*, 664−675.

(13) Zhu, H.; He, X.; Xie, Y.; Guo, S.; Huo, Y.; Wang, W. A Study on the Effect of Coal Metamorphism on the Adsorption Characteristics of a Binary Component System: CO2 and N2. *ACS Omega* **2021**, *6*, 523−532.

(14) Itay, M.; Hill, C. R.; Glasser, D. A study of the low temperature oxidation of coal. *Fuel Process. Technol.* **1989**, *21*, 81−97.

(15) Chen, G.; Ma, X.; Lin, M.; Lin, Y.; Yu, Z. Study on thermochemical kinetic characteristics and interaction during low temperature oxidation of blended coals. *J. Energy Inst.* **2015**, *88*, 221−228.

(16) Fei, Y.; Aziz, A. A.; Nasir, S.; Jackson, W. R.; Marshall, M.; Hulston, J.; Chaffee, A. L. The spontaneous combustion behavior of some low rank coals and a range of dried products. *Fuel* **2009**, *88*, 1650−1655.
(17) Li, Z. Mechanism of Free radical Reactions in spontaneous combustion of coal. *J. China Univ. Min. Technol.* **1996**, *25*, 111−114.
(18) Li, Z.; Kong, B.; Wei, A.; Yang, Y.; Zhou, Y.; Zhang, L. Free radical reaction characteristics of coal low-temperature oxidation and its inhibition method. *Environ. Sci. Pollut. Res.* **2016**, *23*, 23593−23605.
(19) Wei, A. *Experimental Study on Fire Radical Reaction Mechanism of Coal Spontaneous Combustion*; China University of Mining and Technology, 2008.
(20) Wang, D.-M.; Xin, H.; Qi, X.; Dou, G.; Zhong, X. Mechanism and relationships of elementary reactions in spontaneous combustion of coal:The coal oxidation kinetics theory and application. *J. China Coal Soc.* **2014**, *39*, 1667−1674.
(21) Wang, D.-m.; Xin, H.-h.; Qi, X.-y.; Dou, G.-l.; Qi, G.-s.; Ma, L.-y. Reaction pathway of coal oxidation at low temperatures: a model of cyclic chain reactions and kinetic characteristics. *Combust. Flame* **2016**, *163*, 447−460.
(22) Qi, X.; Chen, L.; Xin, H.; Ji, Y.; Bai, C.; Song, R.; Xue, H.; Liu, F. Reaction Mechanism and Thermodynamic Properties of Aliphatic Hydrocarbon Groups during Coal Self-Heating. *Energy Fuels* **2018**, *32*, 10469−10477.
(23) Qi, X.; Xue, H.; Xin, H.; Bai, Z. Quantum chemistry calculation of reaction pathways of carboxyl groups during coal self-heating. *Can. J. Chem.* **2017**, *95*, 824−829.
(24) Qi, X.; Wang, D.; Xue, H.; Jin, L.; Su, B.; Xin, H. Oxidation and Self-Reaction of Carboxyl Groups During Coal Spontaneous Combustion. *Spectrosc. Lett.* **2014**, *48*, 173−178.
(25) Qi, X.; Xue, H.; Xin, H.; Wei, C. Reaction pathways of hydroxyl groups during coal spontaneous combustion. *Can. J. Chem.* **2016**, *94*, 494−500.
(26) Zhang, L.; Li, Z.; He, W.; Li, J.; Qi, X.; Zhu, J.; Zhao, L.; Zhang, X. Study on the change of organic sulfur forms in coal during low-temperature oxidation process. *Fuel* **2018**, *222*, 350−361.
(27) Chen, L.; Qi, X.; Tang, J.; Xin, H.; Liang, Z. Reaction pathways and cyclic chain model of free radicals during coal spontaneous combustion. *Fuel* **2021**, *293*, 120436.
(28) Zhu, H.; Huo, Y.; Fang, S.; He, X.; Wang, W.; Zhang, Y. Quantum Chemical Calculation of Original Aldehyde Groups Reaction Mechanism in Coal Spontaneous Combustion. *Energy Fuels* **2020**, *34*, 14776−14785.
(29) Zhu, H.; Huo, Y.; Wang, W.; He, X.; Fang, S.; Zhang, Y. Quantum chemical calculation of reaction characteristics of hydroxyl at different positions during coal spontaneous combustion. *Process Saf. Environ. Prot.* **2021**, *148*, 624−635.
(30) Qin, B.; Lu, Y.; Li, Y.; Wang, D. Aqueous three-phase foam supported by fly ash for coal spontaneous combustion prevention and control. *Adv. Powder Technol.* **2014**, *25*, 1527−1533.
(31) Tang, Y. Inhibition of Low-Temperature Oxidation of Bituminous Coal Using a Novel Phase-Transition Aerosol. *Energy Fuels* **2016**, *30*, 9303−9309.
(32) Tang, Z.; Xu, G.; Yang, S.; Deng, J.; Xu, Q.; Chang, P. Fire-retardant foam designed to control the spontaneous combustion and the fire of coal: Flame retardant and extinguishing properties. *Powder Technol.* **2021**, *384*, 258−266.
(33) Wang, D.; Dou, G.; Zhong, X.; Xin, H.; Qin, B. An experimental approach to selecting chemical inhibitors to retard the spontaneous combustion of coal. *Fuel* **2014**, *117*, 218−223.
(34) Pandey, J.; Mohalik, N. K.; Mishra, R. K.; Khalkho, A.; Kumar, D.; Singh, V. K. Investigation of the Role of Fire Retardants in Preventing Spontaneous Heating of Coal and Controlling Coal Mine Fires. *Fire Technol.* **2012**, *51*, 227−245.
(35) Watanabe, W. S.; Zhang, D.-k. The effect of inherent and added inorganic matter on low-temperature oxidation reaction of coal. *Fuel Process. Technol.* **2001**, *74*, 145−160.
(36) Wang, X.; Deng, C.; Deng, H. Study of inhibition effect of Ca2+ on phosphorus-contained active groups in coal. *Energy Sources, Part A* **2019**, *43*, 1283−1289.
(37) Slovák, V.; Taraba, B. Urea and CaCl2 as inhibitors of coal low-temperature oxidation. *J. Therm. Anal. Calorim.* **2012**, *110*, 363−367.
(38) Zhan, J. *Roles and Controlling Mechanisms of Additives in coal Oxidation at Low and Moderate Temiaeratures*; University of Science and Technology of China, 2012.
(39) Zhan, J.; Wang, H.-H.; Song, S.-N.; Hu, Y.; Li, J. Role of an additive in retarding coal oxidation at moderate temperatures. *Proc. Combust. Inst.* **2011**, *33*, 2515−2522.
(40) Ma, L.; Wang, D.; Wang, Y.; Xin, H.; Dou, G.; Xu, C. Experimental Investigation on a Sustained Release Type of Inhibitor for Retarding the Spontaneous Combustion of Coal. *Energy Fuels* **2016**, *30*, 8904−8914.
(41) Dou, G.; Wang, D.; Zhong, X.; Qin, B. Effectiveness of catechin and poly(ethylene glycol) at inhibiting the spontaneous combustion of coal. *Fuel Process. Technol.* **2014**, *120*, 123−127.
(42) Xi, Z.; Jin, B.; Shan, Z. Reaction mechanisms involving peroxy radical in the low-temperature oxidation of coal. *Fuel* **2021**, *300*, 120943.
(43) Xi, Z.; Jin, B.; Jin, L.; Li, M.; Li, S. Characteristic analysis of complex antioxidant enzyme inhibitors to inhibit spontaneous combustion of coal. *Fuel* **2020**, *267*, 117301.
(44) Xi, Z.; Li, X.; Xi, K. Study on the reactivity of oxygen-containing functional groups in coal with and without adsorbed water in low-temperature oxidation. *Fuel* **2021**, *304*, 121454.
(45) Li, J.; Li, Z.; Yang, Y.; Kong, B.; Wang, C. Laboratory study on the inhibitory effect of free radical scavenger on coal spontaneous combustion. *Fuel Process. Technol.* **2018**, *171*, 350−360.
(46) Li, J.; Li, Z.; Yang, Y.; Zhang, X.; Yan, D.; Liu, L. Inhibitive Effects of Antioxidants on Coal Spontaneous Combustion. *Energy Fuels* **2017**, *31*, 14180−14190.
(47) Yuan, S. *Fundamental study on reaction mechanism and effect of up grading treatment on spontaneous combustion of lignite*; Zhejiang University, 2018.
(48) Zhu, H.; Huo, Y.; He, X.; Wang, W.; Fang, S.; Zhang, Y. Molecular model construction of Danhou lignite and study on adsorption of CH4 by oxygen functional groups. *Environ. Sci. Pollut. Res.* **2021**, *28*, 25368−25381.
(49) Liu, J.; Jiang, X.; Han, X.; Shen, J.; Zhang, H. Chemical properties of superfine pulverized coals. Part 2. Demineralization effects on free radical characteristics. *Fuel* **2014**, *115*, 685−696.
(50) Jin, B. *Study on reaction mechanism of antioxidant inhibiting coal peroxyradical based on quantum chemical*; Tianjin University of Technology, 2021.
(51) Adamus, A.; Šancer, J.; Guřanová, P.; Zubiček, V. An investigation of the factors associated with interpretation of mine atmosphere for spontaneous combustion in coal mines. *Fuel Process. Technol.* **2011**, *92*, 663−670.
(52) Qin, B.; Dou, G.; Wang, Y.; Xin, H.; Ma, L.; Wang, D. A superabsorbent hydrogel-ascorbic acid composite inhibitor for the suppression of coal oxidation. *Fuel* **2017**, *190*, 129−135.
(53) Tang, Y. Sources of underground CO: Crushing and ambient temperature oxidation of coal. *J. Loss Prev. Process Ind.* **2015**, *38*, 50−57.
(54) Shi, T.; Wang, X.; Deng, J.; Wen, Z. The mechanism at the initial stage of the room-temperature oxidation of coal. *Combust. Flame* **2005**, *140*, 332−345.
(55) Chi, K.; Wang, J.; Ma, L.; Wang, J.; Zhou, C. Synergistic Inhibitory Effect of Free Radical Scavenger/Inorganic Salt Compound Inhibitor on Spontaneous Combustion of Coal. *Combust. Sci. Technol.* **2020**, 1−17.
(56) Yu, S.; Bo, J.; Fengjuan, L. Competitive adsorption of CO2/N2/CH4 onto coal vitrinite macromolecular: Effects of electrostatic interactions and oxygen functionalities. *Fuel* **2019**, *235*, 23−38.
(57) Grimme, S. Density functional theory with London dispersion corrections. *Wiley Interdiscip. Rev.: Comput. Mol. Sci.* **2011**, *1*, 211−228.

https://doi.org/10.1021/acsomega.2c01229
ACS Omega 2022, 7, 18552−18568

(58) Lu, T.; Chen, F. Quantitative analysis of molecular surface based on improved Marching Tetrahedra algorithm. *J. Mol. Graphics Modell.* **2012**, *38*, 314−323.
(59) Deng, J.; Li, Y.; Zhang, Y.; Yang, C.; Zhang, J.; Shi, X. Effects of hydroxyl on oxidation characteristics of side chain active groups in coal. *J. China Coal Soc.* **2020**, *45*, 232−240.
(60) Zhou, C.; Zhang, Y.; Wang, J.; Xue, S.; Wu, J.; Chang, L. Study on the relationship between microscopic functional group and coal mass changes during low-temperature oxidation of coal. *Int. J. Coal Geol.* **2017**, *171*, 212−222.
(61) Hagelin, H.; Murray, J. S.; Politzer, P.; Brinck, T.; Berthelot, M. Family-independent relationships between computed molecular surface quantities and solute hydrogen bond acidity/basicity and solute-induced methanol O-H infrared frequency shifts. *Can. J. Chem.* **1995**, *73*, 483−488.
(62) Xiao-Dong, L.; Tang, Y.; Wang, C.; Zhang, H.; Cheng, X. A DFT Investigation on Hydrogen Adsorption Based on Alkali-metal Organic Complexes. *Chin. J. Struct. Chem.* **2010**, *29*, 1404−1410.

https://doi.org/10.1021/acsomega.2c01229
ACS Omega 2022, 7, 18552−18568